Electronic Supplementary Material (ESI) for Journal of Materials Chemistry C.

SUPPORTING INFORMATION

Molecular Engineering of Enamine-Based Small Organic Compounds as Hole Transporting Materials for Perovskite Solar Cells

Maryte Daskeviciene,[†a] Sanghyun Paek,[†b] Artiom Magomedov,[a] Kyoung Taek Cho,[b] Michael Saliba,[c] Ausra Kizeleviciute,[a] Tadas Malinauskas,[a] Alytis Gruodis,[d] Vygintas Jankauskas,[d] Egidijus Kamarauskas,[d] Mohammad Khaja Nazeeruddin,[*b] and Vytautas Getautis[*a]

Department of Organic Chemistry, Kaunas University of Technology, Radvilenu pl. 19, 50254, Kaunas, Lithuania. E-mail: vytautas.getautis@ktu.lt

Group for Molecular Engineering of Functional Materials, Institute of Chemical Sciences and Engineering, École Polytechnique Fédérale de Lausanne, Rue de l'Industry 17, CH-1951, Sion, Switzerland. E-mail: mdkhaja.nazeeruddin@epfl.ch

Adolphe Merkle Inst, Chemins Verdiers 4, CH-1700 Fribourg, Switzerland

Institute of Chemical Physics Vilnius University, Sauletekio al.3, Vilnius LT-10257, Lithuania

† M. D. and S. P. contributed equally to this work.

General methods

4-aminotriphenylamine was purchased from TCI Europe N.V; 3-amino-9-butylcarbazole was purchased from Chemieliva Pharmaceutical Co., Lt (China); 3,6-diamino-9-(2-ethylhexyl)carbazole was purchased from ABClabtory Scientific Co., Ltd. (China); 3-amino-9-(2-ethyl)hexylcarbazole and 3-amino-6-tert-butylcarbazole from InoChemus Co., Ltd. (Lithuania); Spiro-OMeTAD from Borun New Material Technology Ltd (China). All other chemicals were purchased from Sigma-Aldrich and TCI Europe and used as received without further purification. The ^{1}H and ^{13}C NMR spectra were taken on Bruker Avance III (400 MHz) or Bruker Avance III 700 (700 MHz) spectrometers at room temperature. All the data are given as chemical shifts in δ (ppm). The course of the reactions products was monitored by TLC on ALUGRAM SIL G/UV254 plates and developed with UV light. Silica gel (grade 9385, 230–400 mesh, 60 Å, Aldrich) was used for column chromatography. Elemental analysis was performed with an Exeter Analytical CE-440 elemental analyzer, Model 440 C/H/N/. Electrothermal MEL-TEMP capillary melting point apparatus was used for determination of melting points. UV/Vis spectra were recorded on a PerkinElmer Lambda 35 spectrometer.

Ionization potential measurements

The solid-state ionization potential (I_p) of the layers of the synthesized compounds was measured by the electron photoemission in air method[1–3]. The samples for the ionization potential measurement were prepared by dissolving materials in $CHCl_3$ and were coated on Al plates pre-coated with ~0.5 µm thick methylmethacrylate and methacrylic acid copolymer adhesive layer. The thickness of the transporting material layer was 0.5-1 µm. Usually, photoemission experiments are carried out in a vacuum and high vacuum is one of the main requirements for these measurements. If vacuum is not high enough the sample surface oxidation and gas adsorption are influencing the measurement results. In our case, however, the organic materials investigated are stable enough to oxygen and the measurements may be carried out in the air. The samples were illuminated with monochromatic light from the quartz monochromator with deuterium lamp. The power of the incident light beam was $(2\text{-}5)\cdot 10^{-8}$ W. The negative voltage of –300 V was supplied to the sample substrate. The counter-electrode with the 4.5×15 mm^2 slit for illumination was placed at 8 mm distance from the sample surface. The counter-electrode was connected to the input of the BK2-16 type electrometer, working in the open input regime, for the photocurrent measurement. The 10^{-15}–10^{-12} A strong photocurrent was flowing in the circuit under illumination. The photocurrent I is strongly dependent on the incident light photon energy hν. The $I^{0.5}=f(h\nu)$ dependence was plotted. Usually, the dependence of the photocurrent on incident light quanta energy is well described by a linear relationship between $I^{0.5}$ and hν near the threshold. The linear part of this dependence was extrapolated to the $h\nu$ axis and I_p value was determined as the photon energy at the interception point.

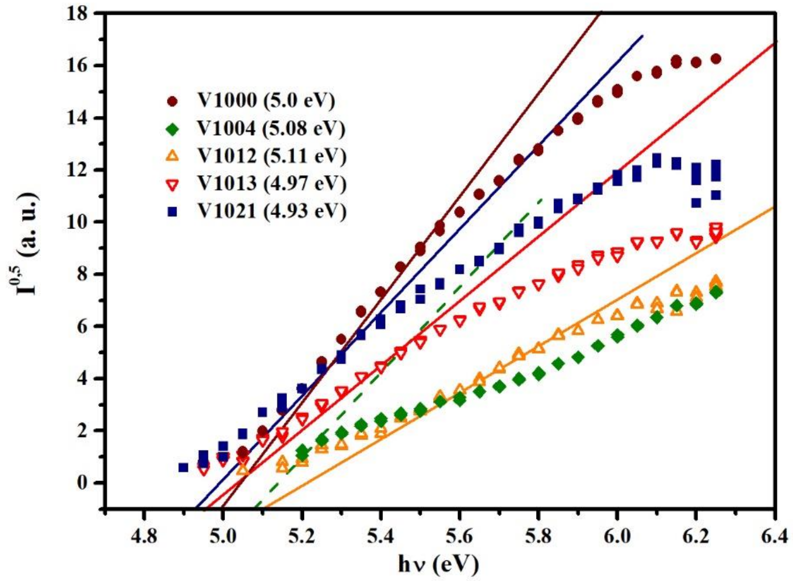

Figure S1. Photoemission in air spectra of the **V1000**, **V1004**, **V1012**, **V1013**, and **V1021**

Hole drift mobility measurements

The samples for the hole mobility measurements were prepared by spin-coating the solutions of the synthesized compounds on the polyester films with a conductive Al layer. The layer thickness was in the range of 5-10 µm. The hole drift mobility was measured by xerographic time of flight technique (XTOF)[4–6]. The electric field was created by positive corona charging. The charge carriers were generated at the layer surface by illumination with pulses of nitrogen laser (pulse duration was 2 ns, wavelength 337 nm). The layer surface potential decrease as a result of pulse illumination was up to 1-5 % of initial potential before illumination. The capacitance probe that was connected to the wide frequency band electrometer measured the speed of the surface potential decrease dU/dt. The transit time t_t was determined by the kink on the curve of the dU/dt transient in double logarithmic scale. The drift mobility was calculated by the formula $\mu=d^2/U_0t_t$, where d is the layer thickness, U_0–the surface potential at the moment of illumination.

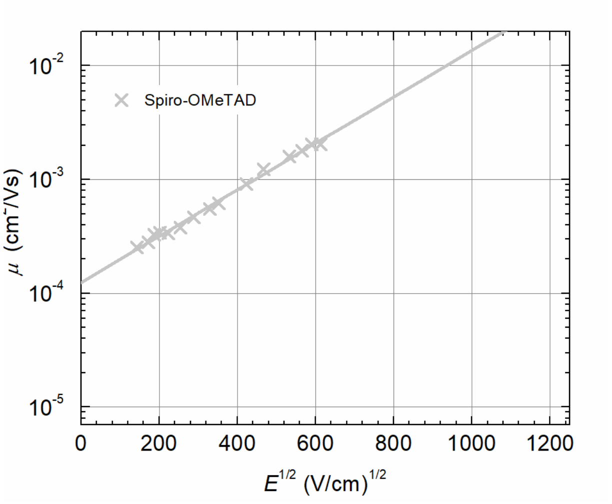

Figure S2. Electric field dependencies of the hole-drift mobility (μ) of the Spiro-OMeTAD

Steady-state photoluminescence

PL spectra was recorded by Luminescence Spectrometer LS55 from Perkin Elmer. 530 nm excitation wavelength was used, and the signal was recorded at 650-900 nm wavelengths.

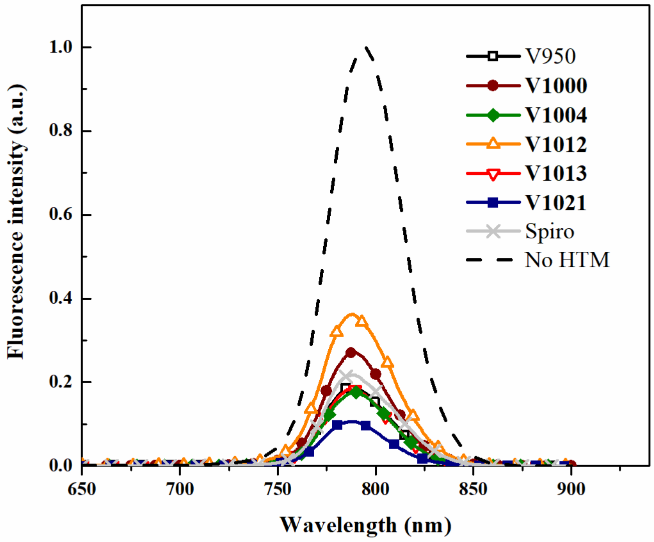

Figure S3. Steady-state photoluminescence (PL) spectra of perovskite films with different HTMs coating

Thermal properties

Differential scanning calorimetry (DSC) was performed on a Q10 calorimeter (TA Instruments) at a scan rate of 10 K·min^{-1} in the nitrogen atmosphere. The glass transition temperatures for the investigated compounds were determined during the second heating scan. Thermogravimetric analysis (TGA) was performed on a Q50 thermogravimetric analyser (TA Instruments) at a scan rate of 10 K·min^{-1}in the nitrogen atmosphere.

Device Fabrication and Testing

Fluorine doped tin oxide (FTO) glass substrates (Nippon sheet glass) were sequentially cleaned with the detergent solution, acetone, and ethanol. And then by spray pyrolysis deposition, a compact TiO_2 layer was coated on the cleaned FTO substrate heated at 450 °C. A precursor solution is prepared by diluting titanium diisopropoxide (Sigma-Aldrich) with ethanol (0.6 mL; 10 mL). Thereafter, we prepared a bilayer electron transport layer with mesoporous TiO_2 and SnO_2. Mesoporous TiO_2 films were prepared using a diluted TiO_2 paste (Dyesol 30 NR-D) solution. Films were prepared by spin-coating and sintered on a hot plate at 500 °C for 30 min. SnO_2 layer was prepared by spin-coating a precursor solution of $SnCl_4$ (Acros) dissolved in water. 0.1 M of $SnCl_4$ aqueous solution was spin-coated and sintered on a hot plate at 180 °C for 1 h. The lead excess $(FAPbI_3)_{0.85}(MAPbBr_3)_{0.15}$ precursor solution was prepared by mixing FAI (1.1 M), PbI_2 (1.15 M), MABr (0.2 M), and $PbBr_2$ (0.2 M) in a mixed solvent of DMF:DMSO = 4:1 (volume ratio). Another solution of $CsPbI_3$ was also prepared as 1.15 M solution in DMF:DMSO (same volume ratio). For triple cations mixed perovskite solution, $(FAPbI_3)_{0.85}(MAPbBr_3)_{0.15}$ and $CsPbI_3$ solutions were mixed as 10 vol% ratio. The perovskite precursor solution was spin coated at 2000 rpm for 10 s, followed by 5000 rpm for 30 s. Trifluorotoluene (110 µL) was dropped on the spinning substrate at the 10 s during the second step. The films were annealed at 100 °C for 90 min in the glove box. The hole-transporting materials were applied from a 40 mM solution in chlorobenzene. Tert-butylpyridine (tBP), tris(2-(1H-pyrazol-1-yl)-4-tert-butylpyridine)cobalt(III) (FK209) and tris(bis(trifluoromethylsulfon-yl)imide) (Li-TFSI) were added as additives. Equimolar amounts of additives were added for all hole transporters: 330 mol% tBP, 50 mol% Li-TFSI from a 1.8 M stock solution in acetonitrile and 3 mol% FK209 from a 0.25 M stock solution in acetonitrile. Finally, 70 nm of Au was deposited by thermal evaporation as the back electrode.

The solar cell measurement was done using commercial solar simulators (Oriel VeraSol-2, AAA class LED). The light intensity was calibrated with a Si reference cell equipped with an IR-cutoff filter (KG3, Newport) and it was recorded before each measurement. Current–voltage characteristics of the cells were obtained by applying an external voltage bias while measuring the current response with a digital source meter (Keithley 2400/2604). The voltage scan rate was 50 mV·s^{-1} and no device preconditioning such as light soaking or forward voltage bias was applied before starting the measurement. The cells were masked with the active area of 0.16 cm^2 to fix the active area and reduce the influence of the scattered light. EQE was measured with IQE200B (Oriel) without bias light.

Hysteresis

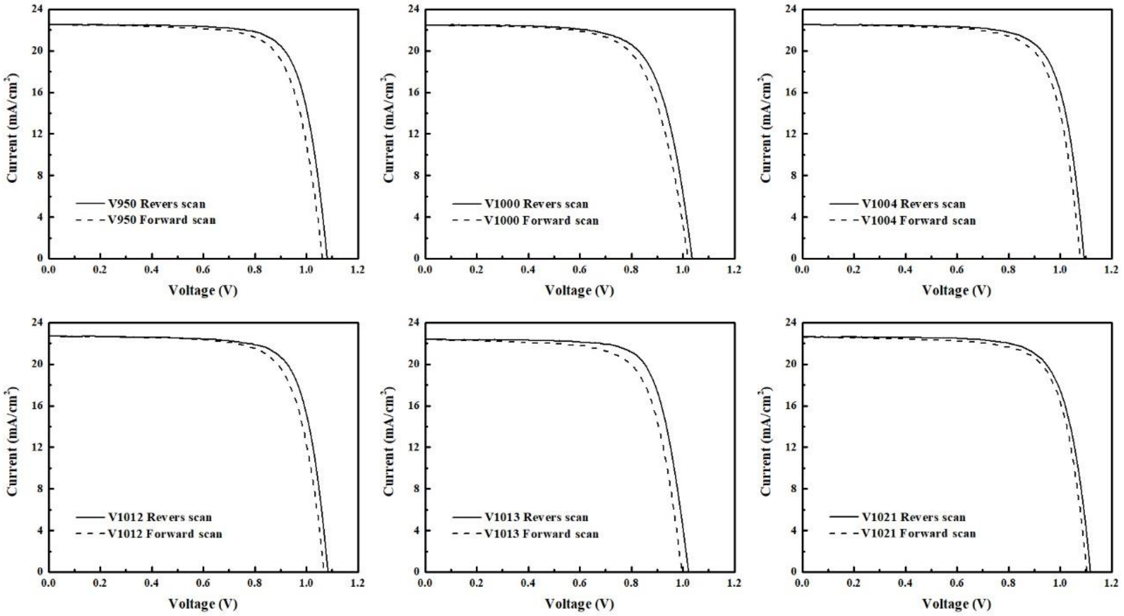

Figure S4. Forward and reverse scans of the best-performing PSC with V950, **V1000**, **V1004**, **V1012**, **V1013**, and **V1021**

Table S1. Solar cell performance parameters, extracted from J-V curves.

HTM	Scan	J_{sc} [mA/cm^2]	V_{oc} [V]	ff	PCE [%]	Average PCE [%]
Spiro_OMeTAD	Reverse	22.5	1.125	0.755	19.10	
V950	Reverse	22.5	1.081	0.757	18.40	17.96
	Forward	22.51	1.062	0.733	17.52	
V1013	Reverse	22.39	1.022	0.747	17.09	16.52
	Forward	22.38	0.995	0.715	15.94	
V1000	Reverse	22.46	1.036	0.71	16.51	16.16
	Forward	22.46	1.020	0.69	15.81	
V1004	Reverse	22.49	1.093	0.757	18.61	18.26
	Forward	22.51	1.079	0.738	17.91	
V1012	Reverse	22.69	1.084	0.756	18.61	18.21
	Forward	22.69	1.068	0.734	17.80	
V1021	Reverse	22.62	1.118	0.752	19.01	18.79
	Forward	22.63	1.104	0.743	18.56	

IPCE

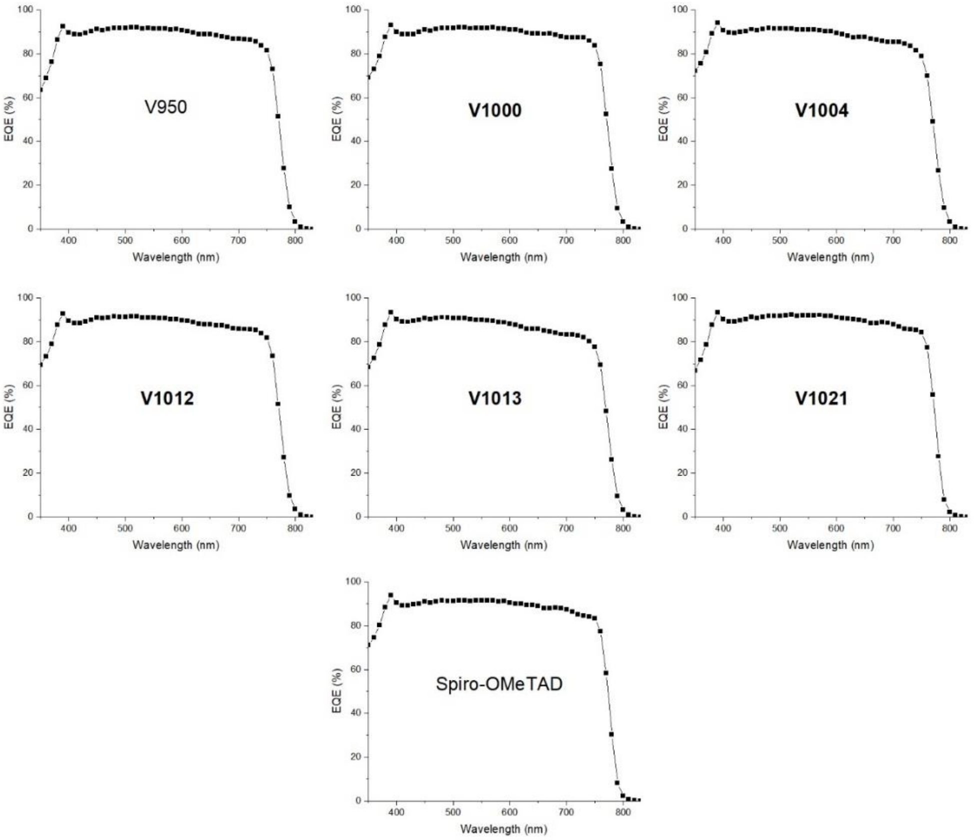

Figure S5. IPCE spectra as a function of the wavelength of monochromatic light of V950, **V1000**, **V1004**, **V1012**, **V1013**, **V1021**, and Spiro-OMeTAD

Statistics

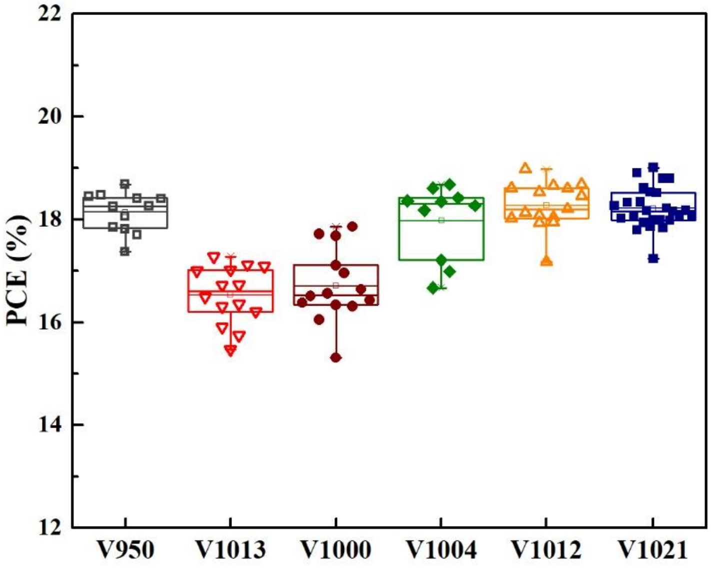

Figure S6 Histograms of the PCEs using various HTMs. A number of devices range from 10 to 26.

Long-term stability

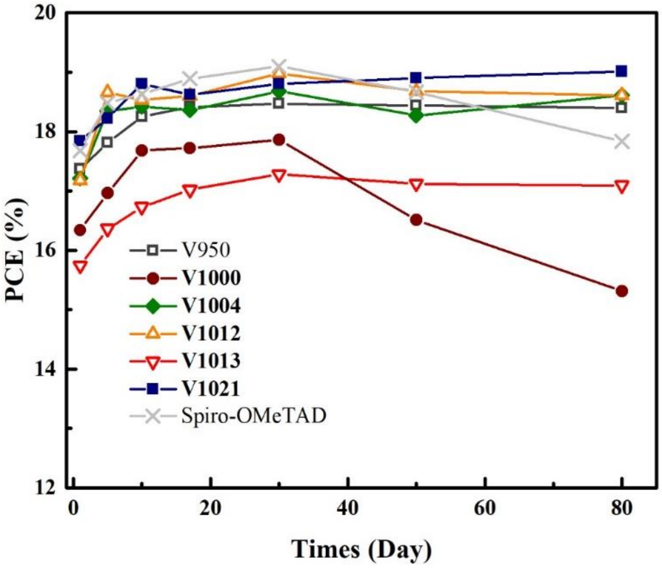

Figure S7. Long-term stability test without encapsulation (relative humidity, ~20%). The device was measured under 1 sunlight illumination and kept the RT in the dark until the next measurement.

Maximum power point tracking

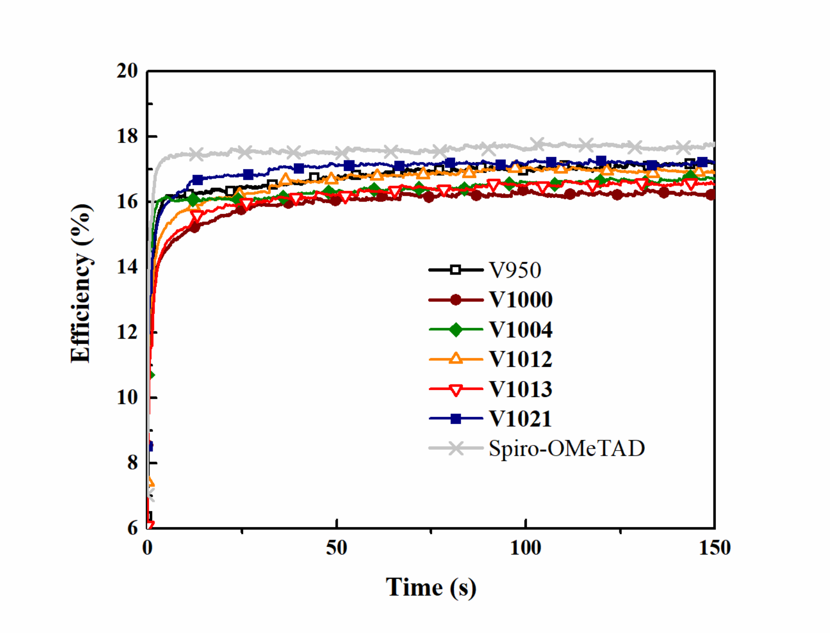

Figure S8. Maximum power point (MPP) tracking of the fresh devices.

Synthesis:

General procedure

To a solution of respective amine (1 mmol) in toluene (5mL + volume of the Dean-Stark trap) (+/-)camphor-10-sulphonic acid (0.9-1.3 mmol) was added and the mixture was heated at reflux for 20 min. Afterwards, 2,2-bis(4-methoxyphenyl)acetaldehyde (2.5-5.0 mmol) was added, and reflux continued using a Dean-Stark trap. After termination of the reaction (TLC, acetone:*n*-hexane, 1:4) the reaction mixture was extracted with ethyl acetate. The organic layer was dried over anhydrous $MgSO_4$, filtered. Then the solvent was removed and the residue was dissolved in the ethanol. The resulting precipitate was filtered off and washed repeatedly with cold ethanol. The product was recrystallized from the mixture of toluene and ethanol (1:2) and dried under vacuum at 40 °C.

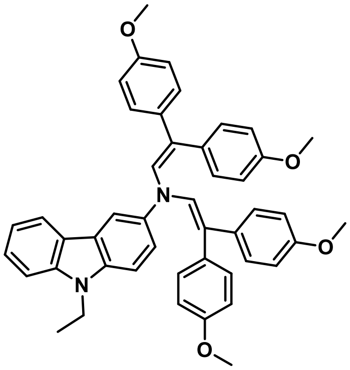

9-ethyl-3-{*N,N*-bis[2,2-bis(4-methoxyphenyl)vinyl]amino}-9*H*-carbazole (V950)

Following general procedure, 3-amino-9-ethyl-9*H*-carbazole (250 mg, 1.19 mmol) was dissolved in toluene (5 mL), (+/-)camphor-10-sulphonic acid (276 mg, 1.19 mmol) was added and the mixture was heated at reflux for 20 min. Afterwards, 2,2-bis(4-methoxyphenyl)acetaldehyde (915 mg, 3.57 mmol) was added, and reflux continued for 2 h more. Yield 590 mg (64 %) m.p.: 226–228 °C.

^{1}H NMR (700 MHz, DMSO-d_6, δ): 8.15 (d, *J* = 7.8 Hz, 1H, 5-H, Ht), 7.80 (s, 1H, 4-H, Ht), 7.58-7.54 (m, 2H, 1,2-H, Ht), 7.44-7.40 (m, 1H 6-H, Ht), 7.24 (d, *J* = 7.0 Hz, 1H, 8-H, Ht), 7.11-7.08 (m, 1H, 7-H, Ht), 6.96 (d, *J* = 8.8 Hz, 4H, *p*-Ph), 6.88 (d, *J* = 9.0 Hz, 4H, *p*-Ph), 6.67 (d, *J* = 9.0 Hz, 4H, *p*-Ph), 6.44 (d, *J* = 8.8 Hz, 4H, *p*-Ph), 5.79 (s, 2H, =CH), 4.42 (q, *J* = 7.0 Hz, 2H, NCH_2), 3.79 (s, 6H, OCH_3), 3.70 (s, 6H, OCH_3), 1.31 (t, *J* = 7.0 Hz, 3H, NCH_3).

^{13}C NMR (176 MHz, DMSO-d_6, δ): 159.06, 139.05, 136.41, 134.49, 132.63, 132.29, 130.65, 129.30, 128.72, 127.61, 126.29, 123.43, 122.33, 121.37, 118.76, 117.16, 114.35, 114.24, 113.53, 110.14, 109.47, 108.72, 55.71 (OCH_3), 55.51 (OCH_3), 37.46 (CH_2), 14.15 (CH_3).

Anal. calcd. for $C_{46}H_{42}N_2O_4$: C, 80.44; H, 6.16; N, 4.08. Found: C, 80.17; H, 6.02; N, 3.91.

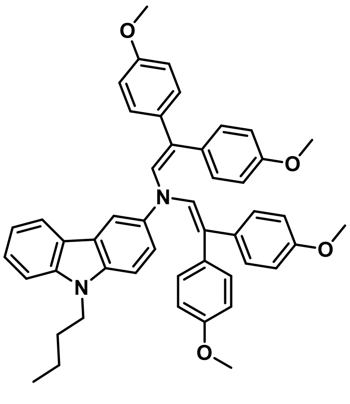

9-butyl-3-{*N,N*-bis[2,2-bis(4-methoxyphenyl)vinyl]amino}-9*H*-carbazole (V1013)

Following general procedure, 3-amino-9-butyl-9*H*-carbazole (1 g, 4.2 mmol) was dissolved in toluene (18 mL), (+/-)camphor-10-sulphonic acid (1 g, 4.3 mmol) was added and the mixture was heated at reflux for 20 min. Afterwards, 2,2-bis(4-methoxyphenyl)acetaldehyde (2.69 g, 10.5 mmol) was added, and reflux continued for 1 h more. Product was purified by column chromatography using 0.5:24.5 v/v THF/*n*-hexane as an eluent and recrystallized from ethanol. Yield: 1.65 g (55%).

^{1}H NMR (400 MHz, $CDCl_3$, δ): 8,05 (d, *J* = 8.9 Hz, 1H, 5-*H*, Ht); 7.81 (s, 1H, 4-*H*, Ht); 7.44 (t, *J* = 7.2 Hz, 1H, 6-*H*, Ht); 7.39-7.33 (m, 1H, 8-*H*, Ht); 7.33 (t, *J* = 7.5 Hz, 2H, 1,2-*H*, Ht); 7.17 (t, *J* = 7.4 Hz, 1H, 7-*H*, Ht); 7.07 (d, *J* = 8.7 Hz, 4H, *p*-Ph); 6.83 (d, *J* = 8.8 Hz, 4H, *p*-Ph); 6.67 (d, *J* =8.8 Hz, 4H, *p*-Ph); 6.54 (d, *J* = 8.8Hz, 4H, *p*-Ph); 5.89 (s, 2H, NCH); 4.30 (t, *J* = 7.1 Hz, 2H, NCH_2); 3.85 (s, 6H, OCH_3); 3.77 (s, 6H, OCH_3); 1.88-1.82 (m, 2H, NCH_2); 1.55 (s, 2H, NCH_2CH_2); 1.44-1.39 (m, 2H, $NCH_2CH_2CH_2$); 0.96 (t, *J* = 7.3 Hz, 3H, CH_3).

^{13}C NMR (75 MHz, $CDCl_3$, δ): 159.0; 158.7; 141.2; 139.2; 136.9; 134.9; 133.2; 130.8; 129.8; 128.9; 127.9; 125.9; 123.7; 122.6; 120.9; 118.5; 116.9; 114.6; 114.0; 113.2; 109.1; 108.8; 55.6 (OCH_3); 55.4 (OCH_3); 43.1 (CH_2); 31.4 (CH_2); 20.7 (CH_2); 14.1 (CH_3).

Anal. calcd. For $C_{48}H_{46}N_2O_4$: C, 80.64; H, 6.49; N, 3.92. Found: C, 80.64; H, 6.41; N, 3.82.

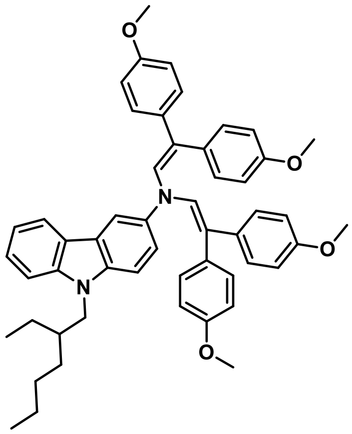

9-(2-ethylhexyl)-3-{*N*,*N*-bis[2,2-bis(4-methoxyphenyl)vinyl]amino}-9*H*-carbazole (V1000)

Following general procedure, 3-amino-9-(2-ethylhexyl)-9*H*-carbazole (1 g, 3.4 mmol) was dissolved in toluene (17 mL), (+/-)camphor-10-sulphonic acid (1 g, 4.3 mmol) was added and the mixture was heated at reflux for 20 min. Afterwards, 2,2-bis(4-methoxyphenyl)acetaldehyde (2.18 g, 8.5 mmol) was added, and reflux continued for 1 h more. Product was purified by column chromatography using 0.5:24.5 v/v acetone/*n*-hexane as an eluent and recrystallized from ethanol. Yield: 1.45 g (57%).

^{1}H NMR (400 MHz, CDCl$_3$, δ): 8.06 (d, *J* = 7.8 Hz, 1H, 5-*H*, Ht); 7.81 (s, 1H, 4-H, Ht); 7.7 (t, *J* = 7.7 Hz, 1H, 6-*H*, Ht); 7.36-7.34 (m, 1H, 8-*H*, Ht); 7.33-7.31 (m, 2H, 1,2-*H*, Ht); 7.17 (t, *J* = 7.4 Hz, 1H, 7-*H*, Ht); 7.07 (d, *J* = 8.4 Hz, 4H, *p*-Ph); 6.84 (d, *J* = 8.4 Hz, 4H, *p*-Ph); 6.67 (d, *J* = 8.5 Hz, 4H, *p*-Ph); 6.54 (d, *J* = 8.5 Hz, 4H, *p*-Ph); 5.89 (s, 2H, NCH); 4.18-4.11 (m, 2H, NCH$_2$); 3.85 (s, 6H, OCH$_3$); 3.77 (s, 6H, OCH$_3$); 2.08-2.05 (m, 1H, NCH$_2$CH); 1.44-1.32 (m, 6H, NCH$_2$(CH$_2$)$_3$); 1.32-1.27 (m, 2H, NCH$_2$CHCH$_2$); 0.93 (t, *J* = 7.4 Hz, 3H, CH$_2$CH$_3$); 0.89 (t, *J* = 7.2 Hz, 3H, CH$_2$CH$_3$).

^{13}C NMR (100 MHz, CDCl$_3$, δ): 159.0; 158.7; 141.7; 139.2; 137.4; 134.9; 133.2; 130.8; 129.8; 128.9; 127.9; 125.8; 123.6; 122.6; 120.9; 118.6; 116.9; 114.; 114.0; 113.2; 109.4; 109.1; 108.7; 55.6 (OCH$_3$); 55.4 (OCH$_3$); 47.7 (CH); 39.7 (CH$_2$); 31.2 (CH$_2$); 29.0 (CH$_2$); 24.5 (CH$_2$); 23.2 (CH$_2$); 14.2 (CH$_3$); 11.1 (CH$_3$).

Anal. calcd. For $C_{52}H_{54}N_2O_4$: C, 81.01; H, 7.06; N, 3.63. Found: C, 80.92; H, 6.99; N, 3.61.

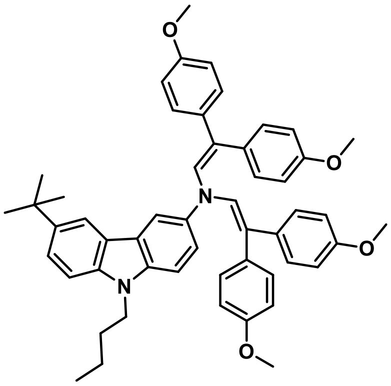

9-butyl-6-(*tert*-butyl)-3-{*N*,*N*-bis[2,2-bis(4-methoxyphenyl)vinyl]amino}-9*H*-carbazole (V1004)

It was prepared from 3-amino-6-(*tert*-butyl)-9-butyl-9*H*-carbazole (1.0 g, 3.4 mmol), (+/-)camphor-10-sulphonic acid (1 g, 4.3 mmol) and 2,2-bis(4-methoxyphenyl)acetaldehyde (2.18 g, 8.5 mmol) in toluene (17 mL) applying the same procedure as for general procedure. The resulting mixture was stirred at reflux for 30 min. Product was purified by column chromatography using 1:24 v/v THF/*n*-hexane as an eluent and further isolated by precipitation of compound 20% THF solution from methanol stock solution. Yield: 1.5 g (57%).

^{1}H NMR (400 MHz, $CDCl_3$, δ): 8.09 (d, *J* = 1.7 Hz, 1H, 5-*H*, Ht); 7.81 (s, 1H, 4-*H*, Ht); 7.54-7.50 (m, 1H, 6-*H*, Ht); 7.33-7.27 (m, 3H, Ht); 7.26 (s, 1H, 7-*H*, Ht); 7.08 (d, *J* = 8.7 Hz, 4H, *p*-Ph); 6.84 (d, *J* = 8.8 Hz, 4H, *p*-Ph); 6.68 (d, *J* = 8.9 Hz, 4H, *p*-Ph); 6.55 (d, *J* = 8.8 Hz, 4H, *p*-Ph); 5.90 (s, 2H, NCH); 4.27 (t, *J* = 7.0 Hz, 2H, NCH_2); 3.85 (s, 6H, OCH_3); 3.78 (s, 6H, OCH_3); 1.43 (s, 9H, $C(CH_3)_3$); 1.47-1.39 (m, 2H, CH_2); 0.96 (t, *J* = 7.3 Hz, 3H, CH_3).

^{13}C NMR (100 MHz, $CDCl_3$, δ): 159.0; 158.7; 141.7; 139.5; 139.4; 138.9; 137.4; 134.9; 133.2; 130.8; 129.6; 129.5; 128.9; 128.1; 123.8; 122.3; 117.2; 116.6; 114.0; 113.2; 109.0; 108.7; 108.2; 55.6 (OCH_3); 55.4 (OCH_3); 43.1 (CH_2); 34.9 (CH_2); 32.2 (CH_2); 31.5 (CH_3); 23.8 (CH_3); 20.8 (CH_3); 14.1 (CH_3).

Anal. calcd. For $C_{52}H_{54}N_2O_4$: C, 81.01; H, 7.06; N, 3.63. Found: C, 81.00; H, 7.02; N, 3.59.

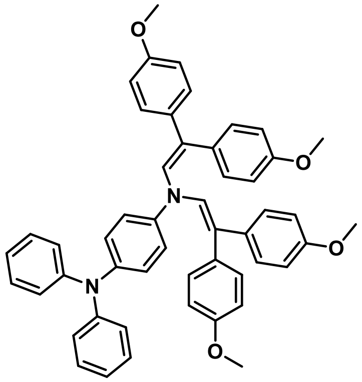

4-{*N*,*N*-bis[2,2-bis(4-methoxyphenyl)vinyl]amino}triphenylamine (V1012)

It was prepared from 4-aminotriphenylamine (1.0 g, 3.8 mmol), (+/-)camphor-10-sulphonic acid (1 g, 4.3 mmol) and 2,2-bis(4-methoxyphenyl)acetaldehyde (2.46 g, 9.6 mmol) in toluene (18 mL) applying the same procedure as for general procedure. The resulting mixture was stirred at reflux for 30 min. Product was purified by column chromatography using 1:24 v/v THF/*n*-hexane as an eluent and further isolated by precipitation of compound 20% THF solution from methanol stock solution._Yield: 1.6 g (58%).

^{1}H NMR (400 MHz, $CDCl_3$, δ): 7.31-7.22 (m, 4H, Ar); 7.15-6.93 (m, 14H, Ar); 6.88 (d, *J* = 8.3 Hz, 4H, *p*-Ph); 6.67 (d, *J* = 8.4 Hz, 4H, *p*-Ph); 6.53 (d, *J* = 8.3 Hz, 4H, *p*-Ph); 5.83 (s, 2H, NCH); 3.89 (s, 6H, OCH_3); 3.78 (s, 6H, OCH_3).

^{13}C NMR (100 MHz, $CDCl_3$, δ): 158.9; 158.6; 148.1; 141.8; 134.4; 132.7; 136.7; 130.2; 129.1; 128.8; 126.4; 123.2; 122.0; 117.9; 114.4; 113.8; 113.0; 99.9; 55.4 (OCH_3); 55.2 (OCH_3).

Anal. calcd. For $C_{50}H_{44}N_2O_4$: C, 81.50; H, 6.02; N, 3.80. Found: C, 81.43; H, 5.92; N, 3.80.

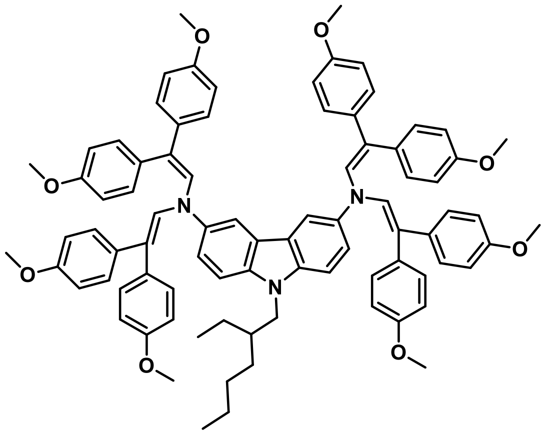

9-(2-ethylhexyl)-3,6-bis{*N*^{3},*N*^{3},*N*^{6},*N*^{6}-tetrakis[2,2-bis(4-methoxyphenyl)vinyl]diamino}-9*H*-carbazole (V1021)

It was prepared from 9-(2-ethylhexyl)-9*H*-carbazole-3,6-diamine (1.0 g, 3.2 mmol), (+/-)camphor-10-sulphonic acid (1 g, 4.3 mmol) and 2,2-bis(4-methoxyphenyl)acetaldehyde (4.1 g, 16 mmol) in toluene (17 mL) applying the same procedure as for general procedure. The resulting mixture was stirred at reflux for 1.5 h. Product was purified by column chromatography using 3:22 v/v acetone/*n*-hexane as an eluent and further isolated by precipitation of compound 20% THF solution from ethanol stock solution. Yield: 2.0 g (49%).

^{1}H NMR (400 MHz, $CDCl_3$, δ): 7.76 (s, 2H, 4,5-*H*, Ht); 7.35-7.26 (m, 4H, 1,2,7,8-*H*, Ht); 7.06 (d, *J* = 8.6 Hz, 8H, *p*-Ph); 6.82 (d, *J* = 8.2 Hz, 8H, *p*-Ph); 6.67-6.60 (m, 8H, *p*-Ph); 6.49 (d, *J* = 8.7 Hz, 8H, *p*-Ph); 5.86 (s, 4H, =CH); 4.11 (d, *J* = 8.4 Hz, 2H, NCH_2); 3.84 (s, 12H, OCH_3); 3.74 (s, 12H, OCH_3); 2.04 (s, 1H, NCH_2CH); 1.45-1.26 (m, 8H, $NCH_2CH(CH_2)_4$); 0.91 (m, 6H, $(CH_3)_2$).

^{13}C NMR (100 MHz, $CDCl_3$, δ): 158.9; 158.6; 144.2; 143.6; 140.6; 134.9; 133.2; 130.9; 129.6; 128.9; 128.0; 123.2; 119.7; 117.7; 117.6; 115.1; 114.6; 113.9; 113.1; 109.3; 89.5; 55.6 (OCH_3); 55.4 (OCH_3); 47.7 (CH); 39.6 (CH_2); 32.8 (CH_2); 31.1 (CH_2); 29.0 (CH_2); 23.3 (CH_2); 14.3 (CH_3); 11.0 (CH_3).

Anal. calcd. For $C_{84}H_{83}N_3O_8$: C, 79.91; H, 6.63; N, 3.33. Found: C, 79.82; H, 6.64; N, 3.31.

Theoretical calculations:

Quantum chemical simulations were performed by means of Gaussian 09 package using density functional theory (DFT) method B3LYP. Optimization of the ground state geometry was done using 6–31G(d) basis set supplemented with polarization functions. Table S2 represents the molecular structures of optimized geometry, Table S3 represents the dipole moments. Atomic distribution of all structures is of non-flat type, the orientation of the enamine branches is a little-bit chaotic due to conformational moieties around [–C–C=] axis.

Table S2. Most probable molecular structures of V950, **V1000**, **V1004**, **V1013**, **V1012** and **V1021** compound. Ground state optimization was performed by Gaussian09 using B3LYP/6-31G(d).

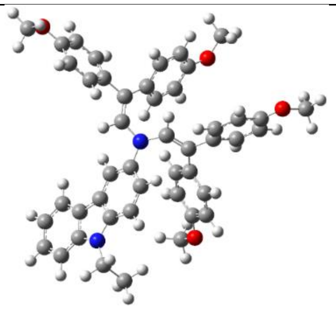 V950	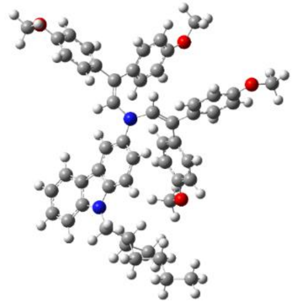 **V1000**
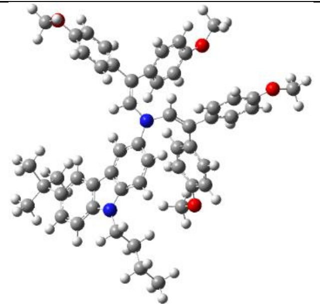 **V1004**	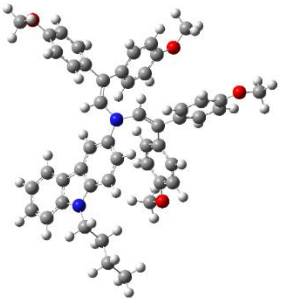 **V1013**
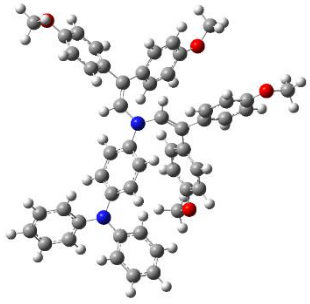 **V1012**	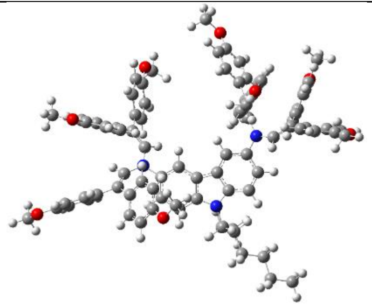 **V1021**

Table S3. Calculated dipole moments (three projections and total) of V950, **V1000**, **V1004**, **V1013**, **V1012** and **V1021** compound. Ground state optimization was performed by *Gaussian09* using B3LYP/6-31G(d).

Compound	d_X, D	d_y, D	d_Z, D	d_{TOTAL}, D
V950	1.08	-0.64	-1.14	1.69
V1000	1.30	-0.98	0.24	1.65
V1004	-1.01	1.37	0.40	1.75
V1013	-1.36	-1.09	0.53	1.83
V1012	-1.39	-0.55	0.57	1.61
V1021	-0.82	0.34	0.11	0.89

Table S4 represents the energies of electronic excitations ($S_0 \rightarrow S_n$) and corresponding oscillator strengths f_n simulated using *Gaussian09* by means of the semiempirical time dependent (TD) method. Transition $S_0 \rightarrow S_1$ is forbidden (f<0.01) for all carbazole-based compounds and partially-allowed (f=0.3) for triphenylamine-based compound (**V1012**), Transition $S_0 \rightarrow S_2$ is partially-allowed (f=0.5) for all compounds except **V1021** (f=0.1).

Table S4. Electronic excitations ($S_0 \rightarrow S_n$) and corresponding oscillator strengths f_n of V950, **V1000**, **V1004**, **V1013**, **V1012,** and **V1021** compound. Excited states S_1, S_2, S_3 were simulated by *Gaussian09* using TD(singlets) routine

Compound	$S_0 \rightarrow S_1$, eV	f_1	$S_0 \rightarrow S_2$, eV	f_2	$S_0 \rightarrow S_3$, eV	f_3
V950	3.06	0.009	3.21	0.555	3.52	0.271
V1000	3.08	0.010	3.21	0.548	3.52	0.277
V1004	3.06	0.010	3.19	0.544	3.52	0.283
V1013	3.07	0.011	3.21	0.545	3.52	0.281
V1012	3.17	0.305	3.27	0.592	3.53	0.095
V1021	2.94	0.099	3.03	0.125	3.15	0.034

Spatial distributions of electron density for the highest occupied molecular orbital (HOMO) and next HOMO, as well as the lowest unoccupied molecular orbital (LUMO) and next LUMO, were obtained using TD routine. Table S5-S10 represent the mentioned distributions for all six compounds.

For single-amino-substituted carbazole-based group (compounds V950, **V1000**, **V1004**, **V1013**), common character of charge redistribution was established (see Table S5-S8). According to simulations using TD(singlets) routine, the population of first excited singlet state S_1 (not allowed transition) could be provided using one-electron excitation of HOMO→LUMO type (see Table S5- S8). Charge redistribution between HOMO (from central amino fragment as the main part and V-shaped fragments as additional part) and LUMO (carbazole fragment) is typical for V950, **V1000**, **V1004**, **V1013** compounds. The population of second excited singlet state S_2 (allowed transition) could be provided using one-electron excitation of HOMO→nextLUMO type. Charge redistribution between HOMO (from central amino fragment as the main part and V-shaped fragments as additional part) and nextLUMO (V-shaped substitute perpendicular to carbazole fragment) is also typical for V950, **V1000**, **V1004**, **V1013** compounds. Also, nextHOMO represents charge distribution along the long axis belonging to two fragments: carbazole and V-shaped substitute. This MO is involved in higher energy transitions.

For three-phenyl-amino-based group (compound **V1012**), the character of charge redistribution differs from the previous one (see Table S9). According to simulations using TD(singlets) routine, the population of first excited singlet state S_1 (partially allowed transition) could be provided using two one-electron excitations of HOMO→LUMO and HOMO→nextLUMO type. Charge redistribution between HOMO (whole molecular distribution) and LUMO (one of both V-shaped fragment) as well as nextLUMO (an area about central amino fragment) is typical for **V1012** compound only. The population of second excited singlet state S_2 (partially allowed transition) could be provided using the same HOMO→LUMO and HOMO→nextLUMO excitations (with the different coefficients). Also, nextHOMO represents charge distribution three-phenyl-amino fragment. This MO is involved in higher energy transitions.

For double-amino-substituted carbazole-based group (compound **V1021**), the similar character of charge redistribution was established (see Table S10). The population of first excited singlet state S_1 (forbidden transition) could be provided using one-electron excitation of HOMO→LUMO type. Charge redistribution between HOMO (from left V-shaped fragment) and LUMO (to right V-shaped fragment) is unique and belongs to the classical CT redistribution. The population of second excited singlet state S_2 (partially allowed transition) could be provided using two one-electron excitations of nextHOMO→LUMO and HOMO→nextLUMO type. In both cases, carbazole fragment plays the role of connector, when charge redistribution between V-shaped fragments from left to right side occurs. It is necessary to point out, that for this case (**V1021**, double-amino-substituted-carbazole-based group), V-shaped substitutes play the role of charge donor as well as of charge acceptor, and type of role belongs on the orientational factor (orientation of V-shaped amino fragments to the carbazole fragment could be changed by occurring the conformational moieties).

Table S5. V950 compound. Spatial distributions of electron density for the HOMO, next HOMO as well as the LUMO and next LUMO. *Gaussian09* using TD(singlets) routine

nextHOMO, 181 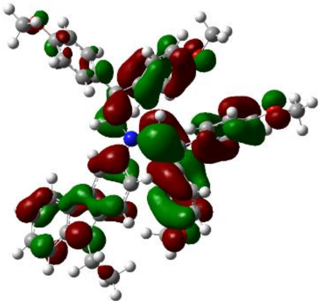	LUMO, 183 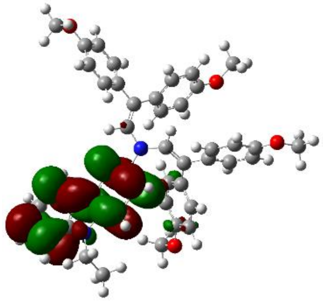
HOMO, 182 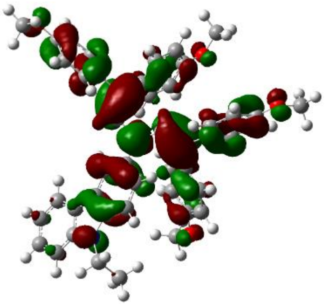	nextLUMO, 184 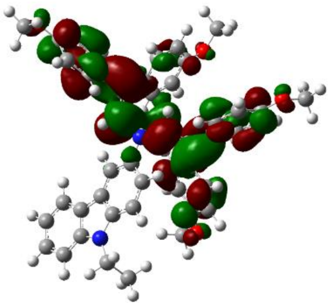

Table S6. **V1000** compound. Spatial distributions of electron density for the HOMO, next HOMO as well as the LUMO and next LUMO. *Gaussian09* using TD(singlets) routine.

nextHOMO, 205 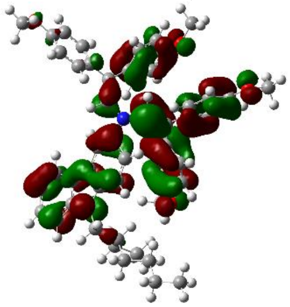	LUMO, 207 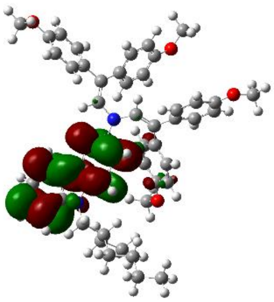
HOMO, 206 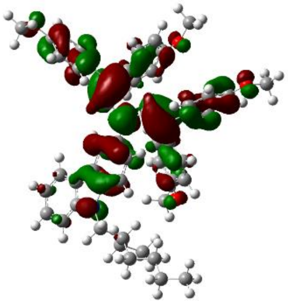	nextLUMO, 208 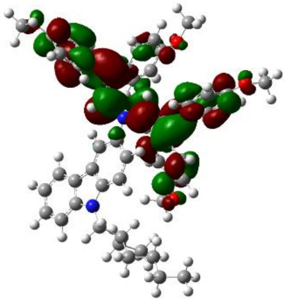

Table S7. **V1004** compound. Spatial distributions of electron density for the HOMO, next HOMO as well as the LUMO and next LUMO. *Gaussian09* using TD(singlets) routine.

nextHOMO, 205 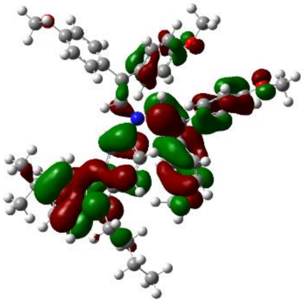	LUMO, 207 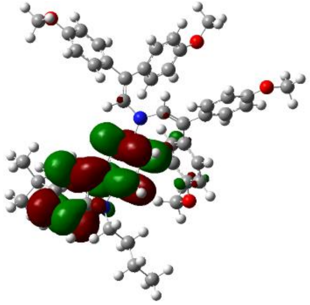
HOMO, 206 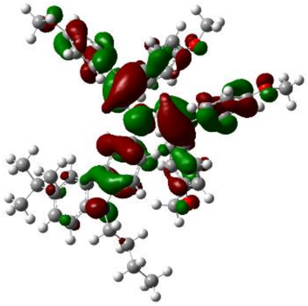	nextLUMO, 208 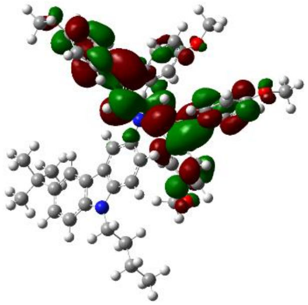

Table S8. **V1013** compound. Spatial distributions of electron density for the HOMO, next HOMO as well as the LUMO and next LUMO. *Gaussian09* using TD(singlets) routine.

nextHOMO, 189 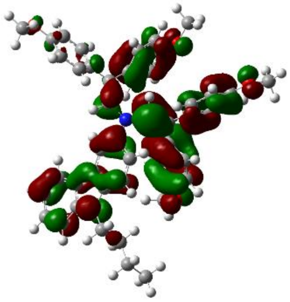	LUMO, 191 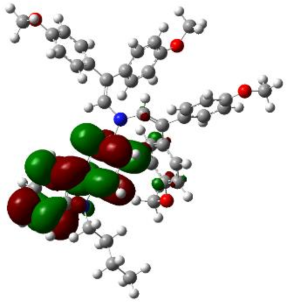
HOMO, 190 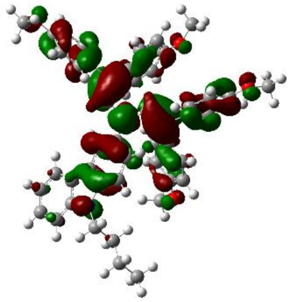	nextLUMO, 192 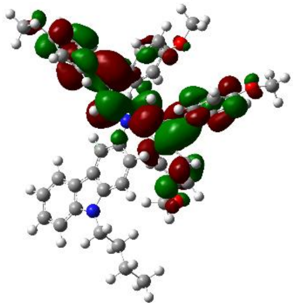

Table S9. **V1012** compound. Spatial distributions of electron density for the HOMO, next HOMO as well as the LUMO and next LUMO. *Gaussian09* using TD(singlets) routine.

nextHOMO, 194 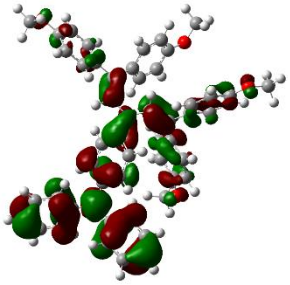	LUMO, 196 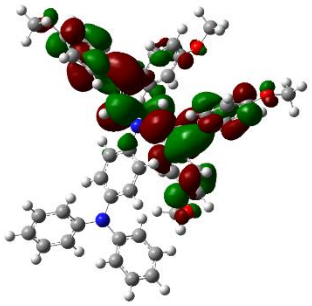
HOMO, 195 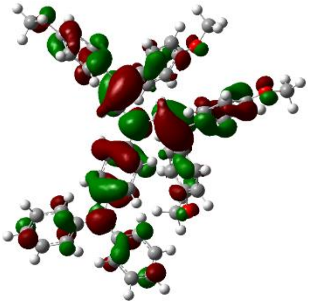	nextLUMO, 197 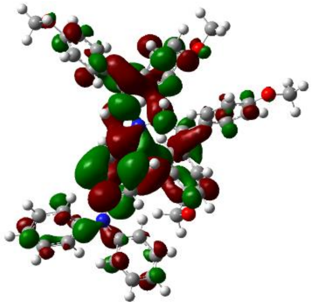

Table S10. **V1021** compound. Spatial distributions of electron density for the HOMO, next HOMO as well as the LUMO and next LUMO. *Gaussian09* using TD(singlets) routine.

nextHOMO, 335 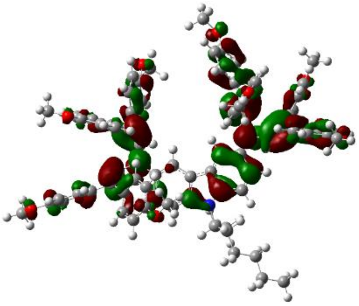	LUMO, 337 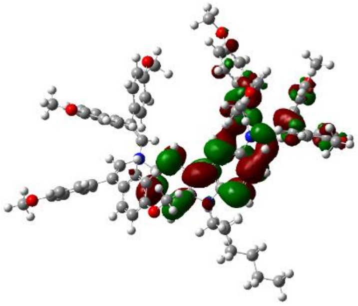
HOMO, 336 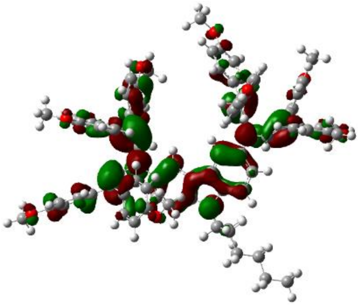	nextLUMO, 338 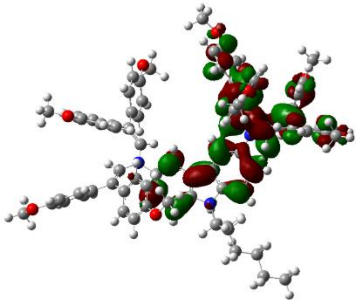

References

1 M. Cordona and L. Ley, *Top. Appl. Phys.*, 1978, **26**, 1.

2 E. Miyamoto, Y. Yamaguchi and M. Yokoyama, *Electrophotography*, 1989, **28**, 364.

3 M. Kirkus, M.-H. Tsai, J. V. Grazulevicius, C.-C. Wu, L.-C. Chi and K.-T. Wong, *Synth. Met.*, 2009, **159**, 729–734.

4 E. Montrimas, V. Gaidelis and A. Pazera, *Lith. J. Phys.*, 1966, **6**, 569–578.

5 A. Y. C. CHAN and C. JUHASZ, *Int. J. Electron.*, 1987, **62**, 625–632.

6 S. M. VAEZI-NEJAD, *Int. J. Electron.*, 1987, **62**, 361–384.